Journal of Electrostatics 69 (2011) 641–647

Contents lists available at SciVerse ScienceDirect

Journal of Electrostatics

journal homepage: www.elsevier.com/locate/elstat

Short communication

Bipolar diffusion charging of high-aspect ratio aerosols

Bon Ki Ku*, Gregory J. Deye, Pramod Kulkarni, Paul A. Baron[1]

Centers for Disease Control and Prevention (CDC), National Institute for Occupational Safety and Health (NIOSH), 4676 Columbia Parkway, MS-R3, Cincinnati, OH 45226, USA

ARTICLE INFO

Article history:
Received 22 February 2011
Received in revised form
30 June 2011
Accepted 8 August 2011
Available online 31 August 2011

Keywords:
Bipolar charging
High-aspect ratio aerosols
Mobility diameter
Aerodynamic diameter
Charging-equivalent diameter

ABSTRACT

Recent studies have raised concerns over applicability of the conventional charging theories to non-spherical particles such as soot aggregates and single-walled carbon nanotube aerosols of complex shape and morphology. It is expected that the role of particle structure and shape on particle diffusion charging characteristics may be significant in the submicron size range for carbon nanotubes (CNTs) and nanofibers (CNFs). In this study, we report experimental data on equilibrium charging characteristics of high-aspect ratio aerosol particles such as CNFs and multi-walled CNTs (MWCNTs) when exposed to a bipolar ion atmosphere. A neutral fraction was measured, i.e., the fraction of particles carrying no electrical charge. A differential mobility analyzer (DMA) was used to classify aerosols, leaving a bipolar radioactive charger to infer the bipolar charging characteristics at different mobility diameters in the submicron size range. The measured neutral fractions for CNF aerosol particles were lower than the corresponding Boltzmann values by 24.4%, 42.0%, and 45.8% for mobility diameters of 400 nm, 600 nm, and 700 nm, respectively, while the neutral fractions for measured aerodynamic diameters of 221 nm, 242 nm, and 254 nm were much lower than those expected by Boltzmann charge distribution, by 43.8%, 63.1%, and 67.3%, respectively. Neutral fractions of spherical particles of polystyrene latex (PSL) and diethylhexyl sebacate (DEHS) particles, measured under identical experimental conditions and procedure, agreed well with the Boltzmann charge distribution. The measured neutral fractions for MWCNT aerosol particles were lower than the corresponding Boltzmann values by 22.3%–25.0% for mobility diameters in the size range from 279 nm to 594 nm. Charging-equivalent diameters of CNF particles correlated well with either mobility diameter or equal-area diameter, which were found to be larger than their mobility or equal-area diameters by up to a factor of 5 in the size range of 400 nm–700 nm, while those of MWCNT particles were larger than the corresponding diameters by a factor of 2 in the size range of 279 nm–594 nm.

Published by Elsevier B.V.

1. Introduction

Bipolar diffusion charging of aerosol particles is of interest in most aerosol measurement applications employing electrical techniques, which require a known, predictable equilibrium charge distribution. Boltzmann and Fuchs charging theories [1,2] have been widely used to describe equilibrium charge distribution. According to Boltzmann theory, the bipolar charge distribution is the result of equilibrium energy exchange between the particles and the surrounding bipolar ions. Diffusion charging of particles depends on the diffusion of ions to the particle surface. The rate at which the ions diffuse to the particle surface depends on the mobility of the ion, the Coulombic force between the ion and the particle, and the attractive image force and van der Waals force. Fuchs proposed a model to include a Coulomb and image potential in the calculations of ion attachment coefficients [2]. These theories assume that particles are spherical in shape.

Many experimental studies have confirmed the validity of these charging theories for spherical particles [3–7]. Of particular importance and interest has been the role of particle structure and shape on particle diffusion charging characteristics. Wen et al. conducted theoretical and experimental investigation of bipolar diffusion charging for fibrous aerosol particles (long chain aggregates) of spherical particles [8,9]. They introduced a concept of charging-equivalent diameter, which was defined as the diameter of a spherical particle that would acquire the same level of charge as that acquired by the non-spherical particles under similar conditions. Their experimental data on fibrous aerosol particles showed close agreement with the Boltzmann charge distribution within 10% when using charging-equivalent diameter. In contrast, some recent studies [6,7,10] have shown that non-spherical soot and carbon nanotube agglomerates could exhibit much higher

* Corresponding author. Tel.: +1 513 841 4147; fax: +1 513 841 4545.
E-mail address: BKu@cdc.gov (B.K. Ku).
[1] Deceased.

0304-3886/$ – see front matter Published by Elsevier B.V.
doi:10.1016/j.elstat.2011.08.006

charging efficiency compared to that predicted by theory. Laframboise and Chang [11] provided a theoretical model of diffusion charging for non-spherical particles to show that for a very elongated spheroid, charge collection might be much more sensitive than in the case of a sphere of the same equatorial radius, which may result in higher particle charging. Biskos et al. [12] showed by using Monte-Carlo simulation that rectangular-shape and elongated chain-agglomerate particles have different unipolar charging behavior, which is 65%–75% higher compared to Fuchs theory. Filippov [13] also reported theoretically that equilibrium charge distribution among aerosol particles of arbitrary shape could differ substantially from the Boltzmann law if particles have high electrical capacitance. Oh et al. [14] demonstrated experimentally that TiO_2 agglomerates with a low fractal dimension have about 30% more charges than spherical particles when they are unipolar-charged. Yu et al. [15] measured the number of charges on asbestos fibers by unipolar diffusion charging to show that the measured values are 5%–10% lower than those calculated from theory.

Tables 1 and 2 summarize all of the studies on unipolar and bipolar diffusion charging of non-spherical particles. Most studies have focused on the effects of particle morphology on charging characteristic. Different particle morphologies such as combustion soot agglomerates, linear-chain aggregates, and nanotube agglomerates were considered for experimental or numerical tests. While unipolar diffusion charging data for these non-spherical particles show high charging efficiency compared to that for spherical particles, bipolar diffusion charging data are scarce. Additional experimental data would be needed to support bipolar diffusion charging of non-spherical particles, especially high-aspect ratio aerosol particles.

This brief communication presents experimental data on bipolar charging characteristics of high-aspect ratio aerosol particles such as carbon nanofiber (CNF) and multi-walled carbon nanotube (MWCNT) aerosol particles. The main objective of this study is to add new data to the existing body of experimental data on non-spherical particle charging. An experimental procedure was used to carefully measure neutral (uncharged) fractions of the CNF and MWCNT aerosols for 300 nm–700 nm in mobility diameter. Carbon nanofibers and multi-walled carbon nanotubes in this study have completely different morphologies from single-walled carbon nanotubes used by Kulkarni et al. [7]. The main difference between our study and Kulkarni et al.'s is that the particles such as CNFs and MWCNTs used in our study have a fibrous shape with high-aspect

Table 1
Summary of previous studies on the effect of non-spherical particle shape on unipolar diffusion charging.

Particle type	Experimental or numerical condition: type of charger	Conclusion	Reference
Rectangular-shaped and elongated chain-aggregate particles dp = 50 nm, AR = 10	Numerical Nt = 5×10^6 ions s cm^{-3}	The Monte-Carlo simulation results showed that mean charges of these particles are 65%–75% higher than the Fuchs model predicted.	Biskos et al. [12]
Titania (TiO_2) agglomerates dp = 6 nm–19 nm Mobility diameter 50 nm–200 nm	No data for Nt	Aggregates with a low fractal dimension have about 30% more charges than spherical particles.	Oh et al. [14]
Fractal-like particles Mobility diameter 10 nm–500 nm	$N = 1.9 \times 10^8$ ions cm^{-3} $t = 0.44$ s Nt = 8.36×10^7 ions s cm^{-3}	Fractal aggregates present higher unipolar charging efficiency (25% higher) than spherical particles with the same electrical mobility diameter.	Ouf and Sillon [16]
Combustion aerosols Mobility diameter 10 nm–300 nm	Nt = 1.97×10^7 ions s cm^{-3}	The mean charge of the monodisperse aerosols is compared with Fuchs' limiting-sphere theory and good agreement is found in most cases.	Biskos et al. [17]
Fibers and platelets d_f = 150 nm, AR = 50 for fibers	Numerical $N = 1 \times 10^7$ ions cm^{-3}, t from 0 to 1 ms	The rate of charge acquisition depends on particle morphology and size. This work did not report results for spherical particles.	Han and Gentry [18]
Soot agglomerates dp = 32 nm Mobility diameter 30 nm–150 nm	Nt ~ 1×10^6 ions s cm^{-3}	It was found that monodisperse soot particles acquire about 15% more charge than compact NaCl particles in the mobility diameter range of 30 nm–150 nm.	Jung and Kittelson [19]
Silver agglomerates dp ~ 20 nm Mobility diameter 20 nm–100 nm	Nt ~ 3×10^6 ions s cm^{-3} Kasper [20]	Silver agglomerates have about 20% more surface area (in turn, charge) than spherical silver particles for mobility diameters below 100 nm.	Ku and Maynard [21]
Soot agglomerates Mobility diameter 30 nm–460 nm	No data for Nt	Soot agglomerate is charged more efficiently than the spherical silver and DOS aerosols. The difference is about ~30% at 100 nm to nearly ~40% at 400 nm	Ntziachristos et al. [22]
Chain aggregate smoke particles Volume equivalent diameter 50 nm–300 nm	No data for Nt	The electrical charge acquired by the aggregates by diffusion is 50%–70% higher than that acquired by spheres of equal volume.	Vomela and Whitby [23]
Asbestos fibers dp = 300 nm, AR = 10	Nt = $0.2–5.0 \times 10^6$ ions s cm^{-3}	The number of charges on asbestos fibers by unipolar diffusion charging is 5%–10% lower than one calculated from theory.	Yu et al. [15]

dp is primary particle diameter consisting of an agglomerate. AR is aspect ratio. *Nt*, where *N* is the ion concentration and *t* is the residence time.

Table 2
Summary of previous studies on the effect of non-spherical particle shapes on bipolar diffusion charging.

Particle type	Experimental or numerical condition: type of charger	Conclusion	Reference
Single-walled carbon nanotube agglomerates Porous envelope shape. Mobility diameter 400 nm–1000 nm	Kr-85	Neutral fractions of SWCNT particles are 30%–53% lower than those Boltzmann and Fuchs theories predicted.	Kulkarni et al. [7]
Soot aggregates dp ~ 20 nm Mobility diameter 15 nm–400 nm	Po-210	Soot charging efficiencies are about 10%–15% higher than those of equal mobility diameter oil droplets in the size range.	Maricq [6]
Soot aggregates dp = 10 nm–30 nm Mobility diameter 100 nm–500 nm	No data for Nt	Charging-equivalent diameter of the soot aggregates is larger than the aggregate mean mobility diameter by a factor of 1.4–3.0.	Karasev et al. [10]
Iron oxide chain aggregates dp = 41 nm–81 nm Aerodynamic diameter 270 nm–450 nm	Kr-85	The Boltzmann distribution is a good approximation for the charge of chain aggregates within 10%.	Wen et al. [9]
Iron oxide chain aggregates dp = 60 nm–130 nm AR = up to 700	Nt = 1×10^7 ions s cm^{-3}	Compared mobility diameter measured by the electrical aerosol analyzer (EAA) with mean mobility equivalent diameters calculated from centrifuge data. The EAA results showed significantly lower diameters (i.e., higher charge) than expected from the model.	Kasper and Shaw [24]
Non-spherical particles. Not specified.	Analytical	The particle capacitance acts as a shape factor, which determines the effective particle radius.	Filippov [13]
Titania (TiO_2) agglomerates dp = 10 nm–20 nm. Compact envelope shape. Mobility diameter 100 nm–800 nm	Kr-85	The bipolar diffusion charging of agglomerate particles is very similar to that of dense spheres of the same mobility with difference of ~5%.	Rogak and Flagan [5]
Elongated spheroid AR = 10	Analytical	For a very elongated spheroid, charge collection will be higher than in the case of a sphere of the same equatorial radius.	Laframboise and Chang [11]
ZnO_2 Aggregates dp ~ 10 nm Mobility diameter 60 nm–200 nm	Kr-85	Charged fraction for ZnO agglomerates behaves approximately like the charged fraction of spherical particles of the same mobility.	Matsoukas and Friedlander [25]

ratio above about 10, but the SWCNTs particles studied by Kulkarni et al. have an envelope shape with low-aspect ratio below about 3 and are heavily agglomerated. Our study is unique in that we used high-aspect ratio fibrous particles and measured the charging characteristics of these particles, which has not been investigated in the previous studies.

2. Experimental

The experimental setup used in this study is shown in Fig. 1. Briefly, the experimental setup consisted of the following components arranged sequentially: i) carbon nanofiber aerosol generation system, ii) batch storage reservoir, iii) differential mobility analyzer (DMA) column to obtain classified aerosol, iv) bipolar test charger (Po-210, 2 mCi) to bring the classified aerosol back to stationary charge equilibrium, v) cylindrical electrostatic precipitator (ESP) that turns on and off to remove charged particles leaving the bipolar charger and determine the neutral fraction of aerosol, followed by vi) condensation particle counter (CPC) that monitored the number concentration of aerosol exiting the ESP. The neutral fraction of the mobility classified aerosol leaving the bipolar charger was determined by taking the ratio of number concentration (of aerosol exiting the ESP) recorded by the CPC with the ESP on and off. Carbon nanofibers (Pyrograf-III, ASI) and multi-walled carbon nanotubes (Mitsui Inc.) were aerosolized by agitation of their powders using a vortex shaker generator [26]. To reduce multiply charged larger particles passing through the DMA column, it was necessary to truncate the supermicron size distribution (>1 μm mobility diameter) of carbon nanofiber aerosols entering the DMA. This was achieved by using a single stage (stage #8) of a micro-orifice uniform deposit impactor (MOUDI) with a cut-off of about 300 nm in aerodynamic diameter (MOUDI, model 110, MSP Corp., Shoreview, MN) [7]. The use of the MOUDI ensured that most of the particles collected in the chamber were not larger than 1000 nm in mobility diameter. This was further confirmed by

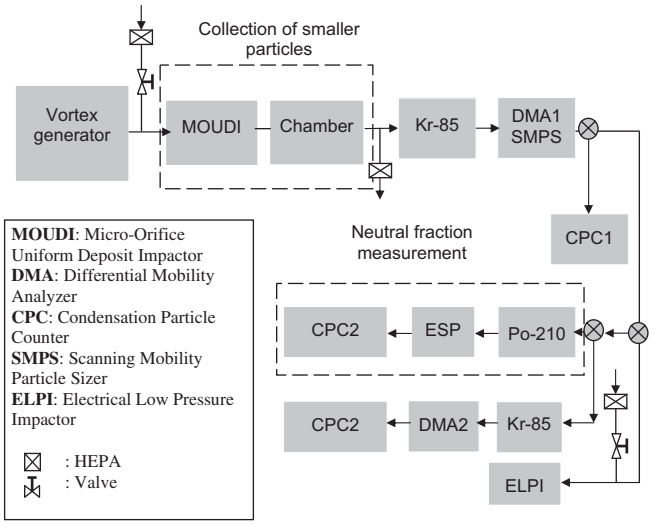

Fig. 1. Experimental setup.

measuring particle size distributions of the aerosol in the batch reservoir using a wide-range particle spectrometer (Model 1000XP; MSP Corp., Shoreview, MN) in the size range of 10 nm to 10 μm. These distributions showed negligible particle concentration beyond 1000 nm. Because some supermicron particles may remain even after most of them are removed by the MOUDI, it was also necessary to obtain a particle size distribution of the aerosol entering the DMA to estimate the fraction of aerosol that acquired

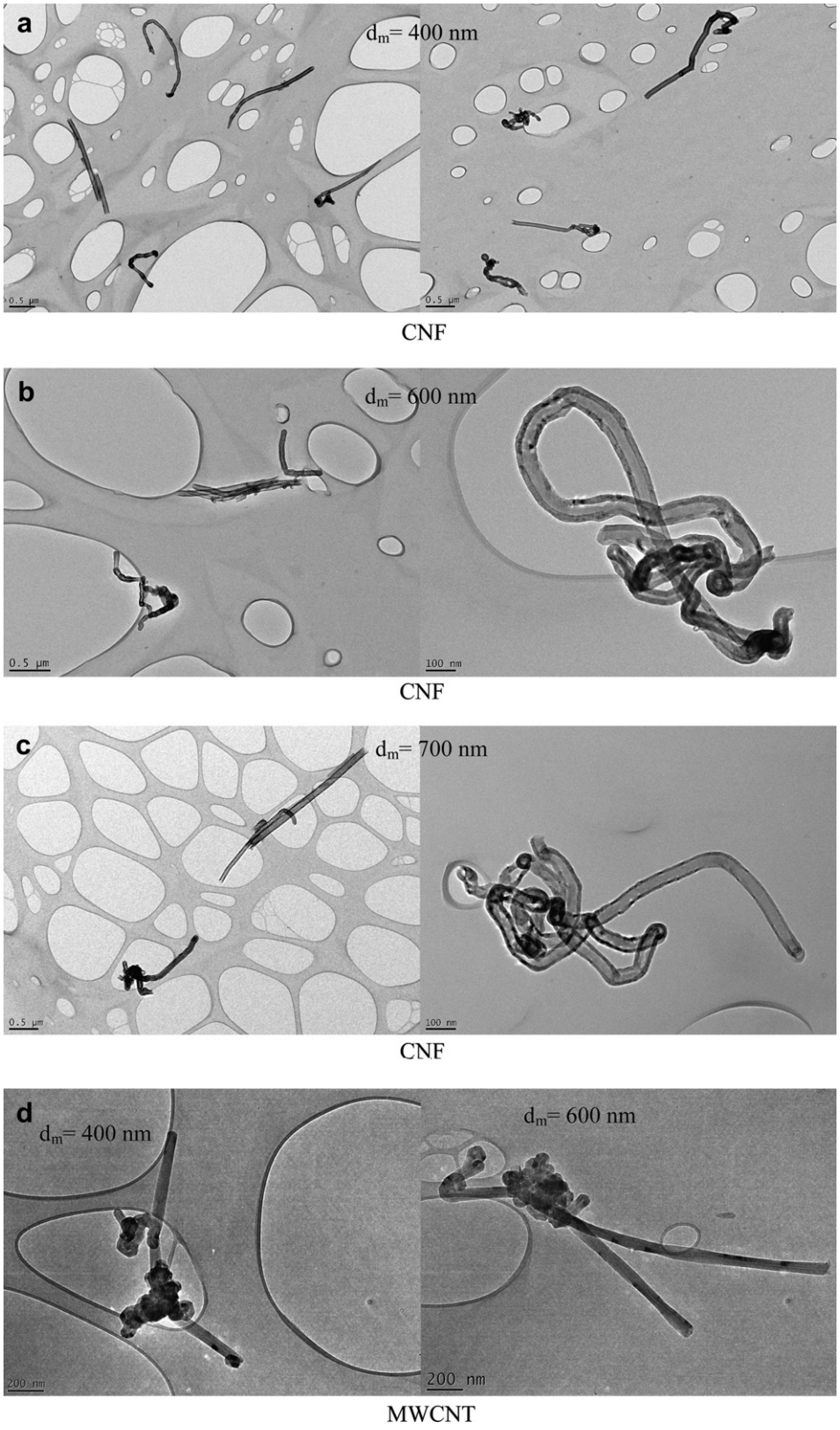

Fig. 2. TEM images of carbon nanofibers (CNFs) and multi-walled carbon nanotubes (MWCNTs) sampled for different mobility diameters: (a) 400 nm (b) 600 nm (c) 700 nm for CNFs and (d) 400 nm & 600 nm for MWCNTs.

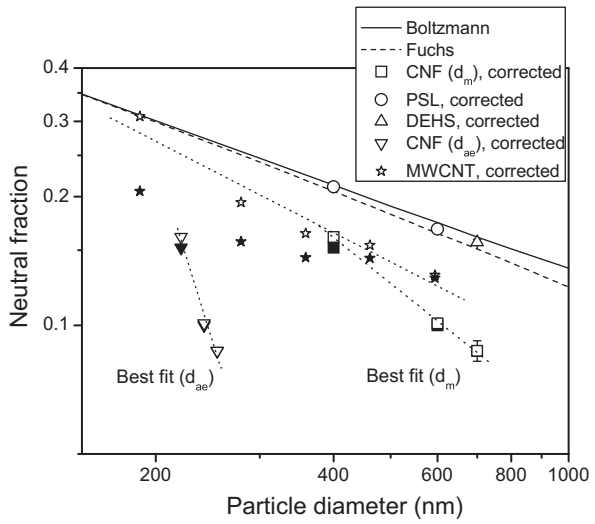

Fig. 3. Corrected neutral fraction of CNF and MWCNT aerosols as a function of mobility diameter (d_m) and aerodynamic diameter (d_{ae}). Error bars on CNF data indicate the standard deviation about an average over three neutral fraction measurements. Filled symbols are uncorrected data for CNF and MWCNT aerosols. Also shown are neutral fractions of spherical particles of PSL and DEHS for comparison.

multiple charges [7]. This was done using a scanning mobility particle sizer (SMPS) to measure the size distribution and then extrapolate the size distribution beyond 1 μm using a lognormal fit. More details on the multiple charge correction procedure are given by Kulkarni et al. [7]. In addition, mean aerodynamic size of classified aerosol from the DMA was measured using an electrical low pressure impactor (ELPI), which requires a sample flow rate of 10 l min^{-1} to investigate the dependence of neutral fraction on different equivalent diameters. To validate the experimental setup, neutral fraction measurement experiments were also performed using the spherical particles at three mobility diameters. Polystyrene latex particles (PSLs, Duke Scientific) of 400 nm and 600 nm diameter were generated by a modified electrospray generator [27], and 700 nm droplets of diethylhexyl sebacate (DEHS) were generated using a condensation monodisperse aerosol generator (Model 3475, TSI Inc) [28].

3. Results and discussion

Fig. 2 shows TEM images of carbon nanofibers and multi-walled carbon nanotubes collected for different mobility diameters. The morphology of particles is clearly fibrous. Carbon nanofibers at low mobility diameters tend to be relatively straight fibers. Carbon nanofibers possess more curly and coiled shapes at higher mobility diameters (600 nm and 700 nm), while multi-walled carbon nanotubes have relatively long and attached tubes at mobility diameter (600 nm). A previous study [26] showed that carbon nanofibers aerosolized by the vortex shaker were formed as fibers attached more randomly to each other and had diameters in the range of 50 nm–200 nm and could be many micrometers long. The carbon nanofiber aerosols generated in this study were relatively less agglomerated because larger nanofiber particles were removed by the MOUDI. For the three mobility diameters studied, the fiber diameters were found to be in the range of 65 nm–120 nm, and the length of fibers in the range of several micrometers. It is worth noting that the degree of agglomeration for CNF particles increased with increasing mobility diameter.

Fig. 3 shows neutral fractions of carbon nanofiber aerosols and spherical particles for three mobility diameters. The error bars on CNF data indicate the standard deviation of about the mean value obtained from three independent neutral fractions measurements.

Table 3
Neutral fractions of carbon nanofibers (CNFs) and multi-walled carbon nanotubes (MWCNTs) measured for different mobility sizes on different dates*.

Mobility diameter (nm)	Neutral fractions					Charging-equivalent diameter[f] (nm)
	Uncorrected	Corrected (±std. dev.)	Spheres[d] – corrected	Boltzmann	Fuchs	
CNF						
400	0.150	–	–	–	–	–
400	0.150	–	–	–	–	–
400	0.157	–	–	–	–	–
400	0.153[a]	–	–	–	–	–
400	**0.152**[b]	**0.161**[c] **(±0.0041)**	**0.211**	**0.213**	**0.206**	**702**
600	0.103	–	–	–	–	–
600	0.100	–	–	–	–	–
600	0.097	–	–	–	–	–
600	**0.0999**[b]	**0.101**[c] **(±0.0028)**	**0.168**	**0.174**	**0.164**	**2100**
700	0.081	–	–	–	–	–
700	0.089	–	–	–	–	–
700	0.090	–	–	–	–	–
700	**0.0868**[b]	**0.0872**[c] **(±0.0048)**	**0.1565**	**0.161**	**0.151**	**3510**
MWCNT						
188	–	**0.308**[e] **(±0.0035)**	–	**0.310**	**0.309**	**191**
279	–	**0.194**[e] **(±0.0040)**	–	**0.255**	**0.250**	**479**
359	–	**0.164**[e] **(±0.0078)**	–	**0.225**	**0.218**	**680**
461	–	**0.154**[e] **(±0.0233)**	–	**0.198**	**0.190**	**772**
594	–	**0.131**[e] **(±0.0205)**	–	**0.175**	**0.165**	**1080**

Bold values are mean values.
*Each neutral fraction datum for each mobility diameter was obtained on a different date to check reproducibility and reliability of the data obtained.
[a] Measured at high electrical field (at high sheath flow) in the DMA.
[b] Mean values of three uncorrected neutral fractions measured for each mobility diameter.
[c] Neutral fractions corrected from the mean values of three uncorrected neutral fractions.
[d] Measured by using PSL and DEHS particles.
[e] These neutral fractions of multi-walled carbon nanotubes (MWCNTs) were measured with a TSI impactor (cut-off size: about 0.7 μm) at the inlet of the SMPS, not with the MOUDI.
[f] Charging-equivalent diameter, defined as a diameter of a spherical particle that results in the same neutral fraction as the carbon nanofiber and MWCNT aerosol, was calculated by interpolation from the Boltzmann charge distribution.

The corrected neutral fractions of carbon nanofiber aerosols are significantly lower than those expected by Boltzmann and Fuchs charge distributions, by about 24.4%, 42.0%, and 45.8% for 400 nm, 600 nm, and 700 nm, respectively. It is worth noting that the neutral fractions of spherical particles in our experiments agree quite well with the Boltzmann and Fuchs values, confirming the validity of our experimental setup and procedures. An artifact from alignment and orientation of CNF particles due to electric field in the DMA might decrease mobility diameter of DMA-classified CNFs if aligned in the electric field. One scenario was tested to determine whether the artifact would in turn have increased the deviation of the neutral fraction from the theory.

For this test, the neutral fraction of carbon nanofibers at 400 nm mobility diameter was obtained at high electric field of 8120 V in the DMA with a sheath flow rate of 6.0 l min^{-1} (all other experiments were performed at 1.7 l min^{-1}). The test revealed that the neutral fractions at high and low electric field for the 400 nm nanofibers were very similar, indicating that the orientation effects were not responsible for the observed deviations from Boltzmann and Fuchs theory.

Fig. 3 also shows neutral fractions of carbon nanofiber aerosols as a function of aerodynamic diameter. The aerodynamic diameters measured are 221 nm, 242 nm, and 254 nm for DMA-classified particles of 400 nm, 600 nm, and 700 nm, respectively. The corrected neutral fractions of carbon nanofiber aerosols based on the aerodynamic diameter are much lower than those expected by Boltzmann charge distribution, by about 43.8%, 63.1%, and 67.3% for 221 nm, 242 nm, and 254 nm, respectively. Compared to the deviation of the neutral fractions based on mobility diameter, the deviation is relatively high when using aerodynamic diameter (the fit of data based on aerodynamic diameter has a higher slope as shown in Fig. 3), indicating that the mobility diameter may be more appropriate in representing the particle charging characteristic. This finding is similar to the result of Wen et al. [9].

Neutral fractions of multi-walled carbon nanotube (MWCNT) aerosols for different mobility diameters are also shown in Fig. 3. Similar to carbon nanofibers, the corrected neutral fractions of carbon nanotube aerosols are lower than those expected by Boltzmann and Fuchs charge distributions by about 22.3%–27.0% in the size range from 300 nm to 600 nm. The neutral fractions of CNF and MWCNT aerosols are summarized in Table 3.

To further investigate whether particle charging can be correlated with a known length scale of the particle such as equal-area diameter, charging-equivalent diameters were first obtained based on the measured neutral fractions. Charging-equivalent diameter, defined as a diameter of a spherical particle that results in the same neutral fraction as the CNF and MWCNT aerosols, was calculated by interpolation from the Boltzmann charge distribution. Charging-equivalent diameters for the CNFs are found to be 702 nm, 2100 nm, and 3510 nm for mobility diameter 400 nm, 600 nm, and 700 nm, respectively, which are higher than mobility diameters by a factor of 1.76–5.01 in the size range of 400 nm–700 nm. The charging-equivalent diameters for the MWCNT particles are larger than the corresponding mobility diameters by a factor of 1.72–1.89 in the size range of 279 nm–594 nm. These results are in reasonable agreement with those of SWCNTs reported by Kulkarni et al. [7] where charging-equivalent diameters were higher than mobility diameter by a factor of 2.85–4.34 in the size range of 400 nm–1000 nm. It should be noted that CNF and MWCNT particles have a fibrous shape with high-aspect ratio more than 10, while the SWCNT particles studied by Kulkarni et al. [7] have an envelope shape consisting of bundles of nanoropes and small aspect ratios (less than 3). Fig. 4 shows charging-equivalent diameter as a function of mobility diameter or equal projected surface-area diameter for CNF and MWCNT aerosols. The equal projected surface area diameter was calculated by TEM image processing of the particles collected for each mobility size using ImageJ, a public domain image analysis program [29]. The ratio of charging-equivalent diameter to mobility diameter (i.e., slope of each fitted line in Fig. 4) is a little bit higher than the ratio of charging-equivalent diameter to equal-area diameter, indicating that the charging-equivalent diameter correlates a little bit better with equal-area diameter. Shahravan et al. [30] reported that a finite charged cylinder in a collisionless plasma collects a charge which is the same as that of an equivalent sphere with the same charge, and that for aspect ratios less than 10, the equivalent sphere diameter is very nearly the same as a sphere diameter of the same area. They also showed that for larger aspect ratios (about 30–40), the sphere of equal area underestimates the charge collected by the cylinder. Our data confirms this fact for CNFs and MWCNTs with high-aspect ratios ranging from 25 to 40 in Fig. 4. We also examined a relationship between charging-equivalent diameter and aspect ratio or theoretical charging-equivalent diameter for CNF aerosol. Theoretical charging-equivalent diameter was calculated with a formula ($d_{qe,\,cal}$ = fiber length/ln(2*aspect ratio)) for a prolate spheroid used by Wen et al. [9]. Fig. 5 shows that charging-equivalent diameter increases with aspect ratio with a good correlation and Fig. 6 shows comparison of measured charging-equivalent diameter with theoretical charging-

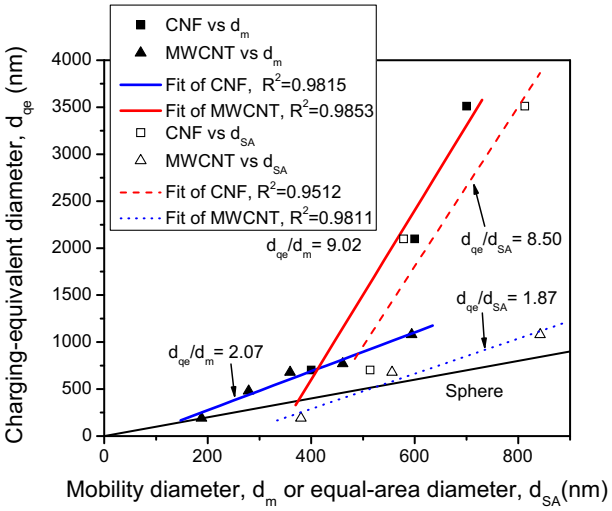

Fig. 4. Charging-equivalent diameter as a function of mobility diameter or equal-area diameter for CNF and MWCNT aerosols. A solid line for spherical particles is included for comparison.

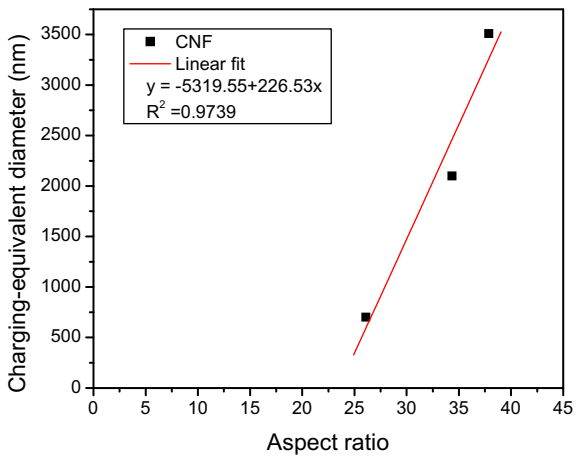

Fig. 5. Charging-equivalent diameter as a function of aspect ratio for CNF aerosol.

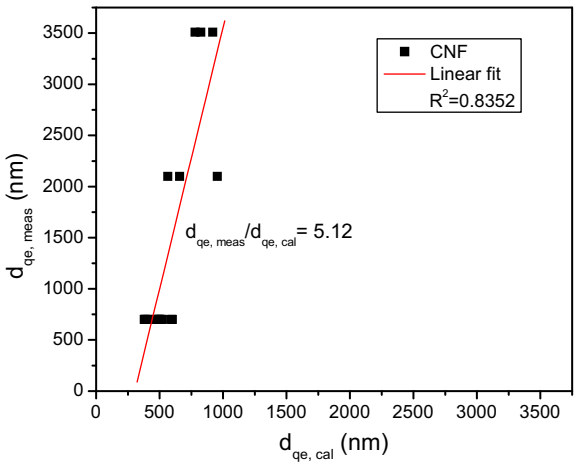

Fig. 6. Comparison of measured charging-equivalent diameter ($d_{qe,meas}$) with calculated charging-equivalent diameter ($d_{qe,\,cal}$) for a prolate spheroid particle proposed by Wen et al. [9].

equivalent diameter. The charging-equivalent diameter correlates well with the theoretical value with a factor of 5. Our results clearly indicate high charging efficiency of high-aspect ratio aerosols compared to spherical particles with the same mobility diameter and that the charging-equivalent diameter correlates well with equal-area diameter.

4. Conclusion

Bipolar diffusion charging behavior of fibrous CNF and MWCNT aerosol particles was found to be different from the Boltzmann and Fuchs charge distribution for spherical particles. The measured neutral fractions for CNF aerosol particles were lower than the corresponding Boltzmann values by 24.4%, 42.0%, and 45.8% for mobility diameters of 400 nm, 600 nm, and 700 nm, respectively, while the neutral fractions for MWCNT aerosol particles were lower than the corresponding Boltzmann values by 22.3%–25.0% for mobility diameters in the size range from 300 nm to 600 nm. Charging-equivalent diameters of CNF particles correlated well with either mobility diameter or equal-area diameter, which were found to be larger than their mobility or equal-area diameters by up to a factor of 5 in the size range of 400 nm–700 nm, while those of MWCNT particles were larger than the corresponding diameters by a factor of 2 in the size range of 279 nm–594 nm. Much more new data on high-aspect ratio particle charging is needed to contribute to better establishing charging behavior of high-aspect ratio particles.

Disclaimer

The mention of any company or product does not constitute an endorsement by the Centers for Disease Control and Prevention. The findings and conclusions in this paper are those of the authors and do not necessarily represent the views of the National Institute for Occupational Safety and Health.

Acknowledgments

This work was funded by the National Institute for Occupational Safety and Health through the National Occupational Research Agenda NTRC funding (CAN 927ZBCL and CAN 927ZJLS). We would like to thank Ellen Galloway for editorial assistance.

References

[1] S.K. Friedlander, Smoke, Dust, and Haze. Oxford University Press, New York, NY, 2000.
[2] N.A. Fuchs, On the stationary charge distribution on aerosol particles in a bipolar ionic atmosphere, Geofisica Pura. E. Applicata 56 (1963) 185–193.
[3] M. Adachi, Y. Kousaka, K. Okuyama, Unipolar and bipolar diffusion charging of ultrafine aerosol particles, J. Aerosol Sci. 16 (1985) 109–123.
[4] W.A. Hoppel, G.M. Frick, Ion-aerosol attachment coefficients and the steady-state charge distribution on aerosols in a bipolar ion environment, Aerosol Sci. Technol. 5 (1986) 1–21.
[5] S.N. Rogak, R.C. Flagan, Bipolar diffusion charging of spheres and agglomerate aerosol particles, J. Aerosol Sci. 23 (1992) 693–710.
[6] M.M. Maricq, Bipolar diffusion charging of soot aggregates, Aerosol Sci. Technol. 42 (2008) 247–254.
[7] P. Kulkarni, G.J. Deye, P.A. Baron, Bipolar diffusion charging characteristics of single-wall carbon nanotube aerosol particles, J. Aerosol Sci. 40 (2009) 164–179.
[8] H.Y. Wen, G.P. Reischl, G. Kasper, Bipolar diffusion charging of fibrous aerosol particles-I. Charging theory, J. Aerosol Sci. 15 (1984a) 89–101.
[9] H.Y. Wen, G.P. Reischl, G. Kasper, Bipolar diffusion charging of fibrous aerosol particles—II. Charge and electrical mobility measurements on linear chain aggregates, J. Aerosol Sci. 15 (1984b) 103–122.
[10] V.V. Karasev, N.A. Ivanova, A.R. Sadykova, N. Kukhareva, A.M. Baklanov, A.A. Onischuk, F.D. Kovalev, S.A. Beresnev, Formation of charged soot aggregates by combustion and pyrolysis: charge distribution and photophoresis, J. Aerosol Sci. 35 (2004) 363–381.
[11] J.G. Laframboise, J.S. Chang, Theory of charge deposition on charged aerosol particles of arbitrary shape, J. Aerosol Sci. 8 (5) (1977) 331–338.
[12] G. Biskos, K. Reavell, N. Collings, Unipolar diffusion charging of aerosol particles in the transition regime, J. Aerosol Sci. 36 (2005) 247–265.
[13] A.V. Filippov, Charge distribution among non-spherical particles in a bipolar ion environment, J. Aerosol Sci. 25 (4) (1994) 611–615.
[14] H. Oh, H. Park, S. Kim, Effects of particle shape on the unipolar diffusion charging of nonspherical particles, Aerosol Sci. Technol. 38 (2004) 1045–1053.
[15] P.Y. Yu, C.C. Wang, J.W. Gentry, Experimental measurement of the rate of unipolar charging of actinolite fibers, J. Aerosol Sci. 18 (1) (1987) 73–85.
[16] F.X. Ouf, P. Sillon, Charging Efficiency of the electrical low pressure impactor's corona charger: influence of the fractal morphology of nanoparticle aggregates and uncertainty analysis of experimental results, Aerosol Sci. Technol. 43 (7) (2009) 685–698.
[17] G. Biskos, E. Mastorakos, N. Collings, Monte-Carlo simulation of unipolar diffusion charging for spherical and non-spherical particles, J. Aerosol Sci. 35 (6) (2004) 707–730.
[18] R.J. Han, J.W. Gentry, Evolution of charge distributions of non-spherical particles undergoing unipolar charging, J. Aerosol Sci. 25 (1994) 499–508.
[19] H. Jung, D.B. Kittelson, Characterization of aerosol surface instruments in transition regime, Aerosol Sci. Technol. 39 (2005) 902–911.
[20] M. Kasper, Personal Communication (2004).
[21] B.K. Ku, A.D. Maynard, Comparing aerosol surface-area measurements of monodisperse ultrafine silver agglomerates by mobility analysis, transmission electron microscopy and diffusion charging, J. Aerosol Sci. 36 (2005) 1108–1124.
[22] L. Ntziachristos, B. Giechaskiel, J. Ristimäki, J. Keskinen, Use of a corona charger for the characterisation of automative exhaust aerosol, J. Aerosol Sci. 35 (2004) 943–963.
[23] R.A. Vomela, K.T. Whitby, The charging and mobility of chain aggregate smoke particles, J. Colloid Interface Sci. 25 (1967) 568–576.
[24] G. Kasper, D.T. Shaw, Comparative size distribution measurements on chain aggregates, Aerosol Sci. Technol. 2 (3) (1983) 369–381.
[25] T. Matsoukas, S.K. Friedlander, Dynamics of aerosol agglomerate formation, J. Colloid Interface Sci. 146 (1991) 495–506.
[26] B.K. Ku, M.S. Emery, A.D. Maynard, M.R. Stolzenburg, P.H. McMurry, In situ structure characterization of airborne carbon nanofibres by a tandem mobility-mass analysis, Nanotechnology 17 (2006) 3613–3621.
[27] B.K. Ku, P. Kulkarni, Morphology of single-wall carbon nanotube aggregates generated by electrospray of aqueous suspensions, J. Nanoparticle Res. 11 (2009) 1393–1403.
[28] B.K. Ku, Determination of the ratio of diffusion charging-based surface area to geometric surface area for spherical particles in the size range of 100–900 nm, J. Aerosol Sci. 41 (2010) 835–847.
[29] ImageJ. http://rsb.info.nih.gov/ij/.
[30] A. Shahravan, C. Lucas, T. Matsoukas, Nanowire charging in collisionless plasma, J. Appl. Phys. 108 (083303) (2010) 1–7.